

# Complex Frequency Fingerprint

Juntao Huang<sup>1</sup>, Kun Ding<sup>2</sup>, Jiangping Hu<sup>3,4,5,\*</sup> and Zhesen Yang<sup>1†</sup>

<sup>1</sup> Department of Physics, Xiamen University, Xiamen 361005, Fujian Province, China

<sup>2</sup> Department of Physics, State Key Laboratory of Surface Physics,

and Key Laboratory of Micro and Nano Photonic Structures (Ministry of Education), Fudan University, Shanghai 200438, China

<sup>3</sup> Beijing National Laboratory for Condensed Matter Physics and Institute of Physics, Chinese Academy of Sciences, Beijing 100190, China

<sup>4</sup> School of Physical Sciences, University of Chinese Academy of Sciences, Beijing 100190, China and

<sup>5</sup> New Cornerstone Science Laboratory, Beijing, 100190, China

(Dated: November 20, 2024)

In this work, we present a novel method called the complex frequency fingerprint (CFF) to detect the complex frequency Green's function,  $G(\omega \in \mathbb{C})$ , in a driven-dissipative system. By utilizing the CFF, we can measure the complex frequency density of states (DOS) and local DOS (LDOS), providing unique insights into the characterization of non-Hermitian systems. By applying our method to systems exhibiting the non-Hermitian skin effect (NHSE), we demonstrate how to use our theory to detect both the non-Hermitian eigenvalues and eigenstates. This offers a distinctive and reliable approach to identifying the presence or absence of NHSE in experimental settings.

**Introduction.**—The Hermiticity of a Hamiltonian is a foundational assumption in quantum mechanics. However, when a system interacts with its external environment, an effective non-Hermitian description may arise [1–4]. Due to the non-orthogonality of eigenstates in a non-Hermitian Hamiltonian, a significant number of eigenstates can become localized at the boundary, leading to the emergence of the non-Hermitian skin effect (NHSE) [5–11]. This phenomenon has been experimentally studied across various physical platforms [3, 4, 12], including photonic systems [13–25], phononic systems [26–38], cold atoms [39, 40], electric circuits [41–53] and mechanical systems [54–60].

From a physical perspective, the presence of the NHSE implies the existence of two distinct responses for the open boundary conditions (OBC) Hamiltonian, as shown in Fig. 1. One corresponds to the Bloch response, where the physical response determined by the OBC Green's function,  $G_{\text{OBC}}$ , can be approximated by the periodic boundary conditions (PBC) Green's function of the Bloch Hamiltonian  $H(k)$ , i.e.,  $G_{\text{OBC}} \simeq G_{\text{PBC}}$ . The other corresponds to the non-Bloch response, indicating that  $G_{\text{OBC}}$ , associated with the non-Bloch Hamiltonian  $H(\beta_{\text{GBZ}})$  [5, 61–75], differs significantly from  $G_{\text{PBC}}$ , i.e.,  $G_{\text{OBC}} \neq G_{\text{PBC}}$  [76, 77]. It can be shown that the non-Bloch response is forbidden in a system lacking NHSE. Thus, the non-Bloch response embodies a unique and fundamental feature of the NHSE.

To detect the non-Bloch response, the driving frequency  $\omega_0$  in the Green's function  $G_{\text{OBC}}(\omega_0)$  is crucial [76, 77]. In Appendix A, we demonstrate that within a purely dissipative system, all Green's functions with real frequencies, i.e.,  $G_{\text{OBC}}(\omega_0 \in \mathbb{R})$ , are attributed to the Bloch response. Therefore, detecting the non-Bloch response necessitates a Green's function with a complex frequency. This raises the fundamental question: how can we detect the complex frequency Green's function?

In this work, we introduce the concept of the complex frequency fingerprint (CFF), as shown in Fig. 1, to systematically detect the non-Bloch response. Starting with a driven-

dissipative bosonic quantum system, our analysis of the quantum master equation reveals that the time evolution of the field operator's mean value is governed by a dissipative non-Hermitian Hamiltonian with an external drive. The CFF is defined based on the time-dependent response function. By employing the CFF, we demonstrate that the complex frequency Green's function, i.e.,  $G(\omega \in \mathbb{C})$ , can be detected experimentally, providing information on the complex frequency DOS, LDOS, and propagators. As applications, we showcase the utility of the CFF in detecting three key physical quantities in non-Hermitian physics: the non-Hermitian eigenvalues (spectrum), eigenstates, and impurity bound state. Our theory offers novel insights into exploring the physical response induced by the NHSE.

**Driven-dissipative quantum system.**—To investigate the non-Bloch response in realistic systems, we simulate our system as a driven-dissipative quantum system, with its dynamics governed by the following quantum master equation [78–81]

$$\frac{d\hat{\rho}(t)}{dt} = -i[\hat{H}(t), \hat{\rho}(t)] + \sum_{m=1}^N \kappa_m \hat{\mathcal{L}}_m[\hat{\rho}(t)], \quad (1)$$

where  $\hat{H}(t) = \sum_{mn} t_{mn} \hat{a}_m^\dagger \hat{a}_n + \sum_m (\hat{a}_m^\dagger F_m(t) + F_m^*(t) \hat{a}_m)$  is the Hermitian driven Hamiltonian with  $t_{mn} = t_{nm}^*$ ,  $\hat{a}_m^\dagger$ ,

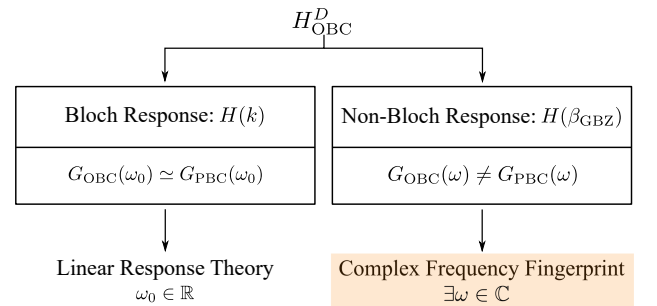


FIG. 1. The comparison between Bloch and non-Bloch responses is illustrated. Here,  $D$  in  $H_{\text{OBC}}^D$  represents the dissipative system.

$\hat{a}_m$ ,  $\hat{\rho}(t)$  and  $F_m(t)$  denoting the hopping parameter, creation and annihilation operators of the bosonic modes, density matrix, and external driving field, respectively.

$$\hat{\mathcal{L}}_m[\hat{\rho}(t)] = \hat{a}_m\hat{\rho}(t)\hat{a}_m^\dagger - \frac{1}{2}\{\hat{a}_m^\dagger\hat{a}_m, \hat{\rho}(t)\}, \quad (2)$$

is the dissipative superoperator, and  $\kappa_m$  in Eq. 1 represents the local damping rate for each bosonic mode.

In Appendix B, we will demonstrate that the equation of motion for the mean value of the single-particle operator satisfies

$$i\frac{d\langle\hat{\mathbf{a}}(t)\rangle}{dt} = H_{\text{NH}}\langle\hat{\mathbf{a}}(t)\rangle + \mathbf{F}(t), \quad (3)$$

where  $[H_{\text{NH}}]_{mn} = t_{mn} - \frac{i}{2}\kappa_m\delta_{mn}$  is an effective non-Hermitian Hamiltonian written in first-quantized form,  $\langle\hat{\mathbf{a}}(t)\rangle = \{\text{Tr}[\hat{a}_1\hat{\rho}(t)], \dots, \text{Tr}[\hat{a}_N\hat{\rho}(t)]\}^T$ , and  $\mathbf{F}(t) = \{F_1(t), \dots, F_N(t)\}^T$ . Notably, (i) no approximation is made in the process of deriving Eq. 3 from Eq. 1, and the appearance of  $H_{\text{NH}}$  is exact; (ii) Eq. 3 is also equivalent to the dynamic equation in classical wave systems [82–86], enabling the application of all conclusions from this work to classical wave systems; (iii) a general solution of Eq. 3 will be provided in the appendix; (iv) in experimental settings, the quantity  $\langle\hat{\mathbf{a}}(t)\rangle$  is a physical observable enabling the simultaneous measurement of both its amplitude and phase [13–38, 41–60].

**Complex frequency fingerprint.**—Now, assume a harmonic external driving characterized by:

$$\mathbf{F}_{\omega_0}(t) = \theta(t)e^{-i\omega_0 t}\{F_1(0), \dots, F_N(0)\}^T, \quad \omega_0 \in \mathbb{R} \quad (4)$$

where  $\omega_0$  is the driving frequency,  $\theta(t)$  is the step function, and  $F_i(0)$  is the driving amplitude at site  $i$ . Then, the solution for  $\langle\hat{\mathbf{a}}(t)\rangle$  is expressed in the form of the response function:

$$\langle\hat{\mathbf{a}}(t)\rangle_{\omega_0} = \chi_{\omega_0}(t)\mathbf{F}_{\omega_0}(t). \quad (5)$$

As derived in Appendix C, the response function  $\chi_{\omega_0}(t)$  is expressed as:

$$\begin{aligned} [\chi_{\omega_0}(t)]_{mn} &= [G(\omega_0)]_{mn} - [G(\omega_0)e^{-i(H_{\text{NH}}-\omega_0)t}]_{mn} \\ &+ [e^{-i(H_{\text{NH}}-\omega_0)t}]_{mn}\langle\hat{a}_n(0)\rangle/F_n(0), \end{aligned} \quad (6)$$

with  $G(\omega_0)$  representing the real frequency single-particle Green's function, i.e.,  $G(\omega_0) = 1/(\omega_0 - H_{\text{NH}})$ . Notably, since the system is dissipative, the time evolution contribution in Eq. 6 will decay to zero as  $t \rightarrow \infty$ , which leads to:

$$\lim_{t \rightarrow \infty} \chi_{\omega_0}(t) = G(\omega_0). \quad (7)$$

Therefore, the steady-state response to the real frequency driving is equal to the corresponding Green's function, representing the traditional approach for Green's function detection in experiments.

It is essential to highlight that the solutions presented in Eq. 5 and Eq. 6 can be extended to complex driving frequencies, i.e.,  $\omega_0 \in \mathbb{C}$ . However, this method is not suitable

for detecting the complex frequency Green's function, i.e.,  $G(\omega_0 \in \mathbb{C})$ . The reason is that if  $\text{Im}(E_n - \omega_0) > 0$ , indicating a system with virtual gain [87–96], the time evolution contribution in Eq. 6 may diverge as  $t$  approaches infinity, failing to provide information on  $G(\omega_0 \in \mathbb{C})$ .

Our strategy for detecting the complex frequency Green's function is based on the following observation: Eq. 7 reveals that the non-Hermitian Hamiltonian  $H_{\text{NH}}$  can be directly obtained from the response function, i.e.,  $\lim_{t \rightarrow \infty} [\omega_0 - \chi_{\omega_0}^{-1}(t)] = H_{\text{NH}}$ . Consequently, we can define the CFF with a complex frequency as:

$$\mathcal{G}_{\omega_0}(\omega \in \mathbb{C}; t) = \frac{1}{\omega - \omega_0 + \chi_{\omega_0}^{-1}(t)}, \quad (8)$$

and prove that as  $t$  approaches infinity, the CFF converges to the complex frequency Green's function of our non-Hermitian Hamiltonian, i.e.,

$$\lim_{t \rightarrow \infty} \mathcal{G}_{\omega_0}(\omega \in \mathbb{C}; t) = G(\omega \in \mathbb{C}) = \frac{1}{\omega - H_{\text{NH}}}. \quad (9)$$

Hence, in experimental settings, once the response function  $\chi_{\omega_0}(t)$  is obtained, the CFF can be calculated directly for any given  $\omega \in \mathbb{C}$ . Furthermore, if the system reaches a steady state ( $t > t_s$  as explained in Appendix D), the CFF can be reasonably approximated as the complex frequency Green's function as we want, i.e.,  $\mathcal{G}_{\omega_0}(\omega \in \mathbb{C}; t > t_s) \simeq G(\omega \in \mathbb{C})$ . This is the central conclusion of our manuscript. Additionally, since  $H_{\text{NH}}$  remains independent of  $\omega_0$ , the CFF remains invariant under the choice of  $\omega_0$  as  $t$  approaches infinity. Therefore, we simplify our notation in subsequent discussions by omitting the subscript  $\omega_0$ , i.e.,

$$\mathcal{G}_{\omega_0}(\omega \in \mathbb{C}; t) \rightarrow \mathcal{G}(\omega \in \mathbb{C}; t). \quad (10)$$

Moreover, we assume  $\langle\hat{\mathbf{a}}(0)\rangle = 0$  in the following discussion, which does not affect our qualitative conclusions.

**Application to the non-Bloch response: spectrum**—Now we will elucidate the relationship between the CFF and the non-Bloch response, which can be used to detect non-Hermitian eigenvalues, eigenstates, and impurity bound states.

To begin, we define the complex frequency DOS of the CFF to characterize the non-Hermitian eigenvalues:

$$\mathcal{D}(\omega \in \mathbb{C}; t) = -\frac{1}{N\pi} \text{Im Tr } \mathcal{G}(\omega \in \mathbb{C}; t). \quad (11)$$

As  $t$  approaches infinity, this quantity converges to the conventional complex frequency DOS of the non-Hermitian Hamiltonian:

$$\begin{aligned} \lim_{t \rightarrow \infty} \mathcal{D}(\omega \in \mathbb{C}; t) &= D(\omega \in \mathbb{C}) \\ &= -\frac{1}{N\pi} \text{Im Tr } \frac{1}{\omega - H_{\text{NH}}}. \end{aligned} \quad (12)$$

Therefore, as  $\omega$  approaches an eigenvalue of  $H_{\text{NH}}$ , say  $E_n$ ,  $\mathcal{D}(\omega \in \mathbb{C}; t)$  diverges, providing the spectral signature of the

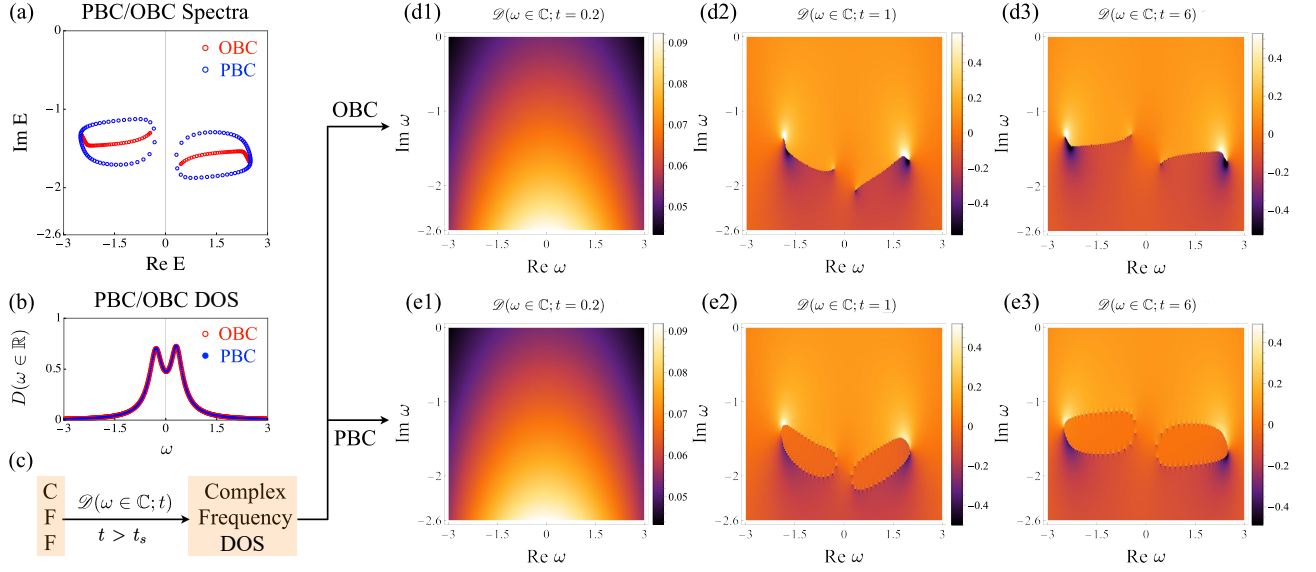


FIG. 2. (a) The PBC and OBC spectra of Eq. 15. (b) The PBC and OBC DOS in the real frequency domain, i.e.  $D(\omega \in \mathbb{R}) = -(1/\pi N) \text{Im Tr} \frac{1}{\omega - H_{\text{NH}}}$ . (c) A schematic illustrating the detection of the complex frequency DOS based on the CFF. (d1)-(d3)  $\mathcal{D}(\omega \in \mathbb{C}; t)$  under OBC for  $t = 0.2, 1$  and  $6$  respectively. (e1)-(e3)  $\mathcal{D}(\omega \in \mathbb{C}; t)$  under PBC for  $t = 0.2, 1$  and  $6$  respectively. Here, the parameters are selected as  $t_1 = 1.5, t_2 = 1, \mu = 0.3, \gamma_0 = 3, \gamma_z = 1, \lambda = 1, \omega_0 = 0$  and  $N = 50$  for both OBC and PBC.

eigenvalues. It is important to note that the complex frequency DOS,  $D(\omega \in \mathbb{C})$ , differs from the spectral DOS of the non-Hermitian Hamiltonian  $H_{\text{NH}}$ , which is defined as:

$$\rho(\omega) = \frac{1}{N} \sum_n \delta(\text{Re } \omega - \text{Re } E_n) \delta(\text{Im } \omega - \text{Im } E_n). \quad (13)$$

where  $E_n$  denotes the  $n$ -th eigenvalue of  $H_{\text{NH}}$  under either PBC or OBC. The CFF can also detect  $\rho(\omega)$ , as elaborated in Appendix D.

The relation between  $D(\omega \in \mathbb{C})$  and  $\rho(\omega)$  is that if we regard  $E_n$  as an electric charge in the two-dimensional complex frequency plane, then  $\rho(\omega)$  corresponds to the charge density, and  $D(\omega \in \mathbb{C})$  serves as the  $y$  component of the electric field:

$$\mathcal{E} = \frac{1}{2\pi N} \sum_n \frac{(\text{Re } \omega - \text{Re } E_n, \text{Im } \omega - \text{Im } E_n)}{|\omega - E_n|^2}, \quad (14)$$

which resembles the electric field arising from a line of charge, as elucidated in Appendix D.

Our numerical example for detecting the spectrum is based on the spinless model proposed in Ref. [97]:

$$H_{\text{NH}}(\mathbf{k}) = (t_1 + t_2 \cos k) \sigma_x + t_2 \sin k \sigma_y + (\lambda \sin k + \mu) \sigma_z - i(\gamma_0 \sigma_0 + \gamma_z \sigma_z)/2. \quad (15)$$

Here  $\gamma_1 = (\gamma_0 + \gamma_z)/2$  and  $\gamma_2 = (\gamma_0 - \gamma_z)/2$  represent the onsite dissipation at the A and B sub-lattices, respectively.

When  $\gamma_1 \neq \gamma_2$ , the NHSE appears, which leads to a significant distinction between the OBC and PBC spectra, as shown in Fig. 2 (a). Since the system is purely dissipative, the real frequency DOS, i.e.,  $D(\omega \in \mathbb{R})$ , shows no differences under

PBC and OBC, which belongs to the Bloch response, as illustrated in Fig. 2 (b). For comparison, the CFF method for detecting the complex frequency DOS is illustrated in Fig. 2 (c), with the corresponding results presented in Fig. 2 (d1)-(d3) and (e1)-(e3) for OBC and PBC, respectively. The plots of  $\mathcal{D}(\omega \in \mathbb{C}; t)$  for OBC and PBC range from  $t = 0.2$  to  $1$  and  $6$ . Here,  $\omega_0$  is chosen to be  $0$ , which does not impact the final result. As time evolves, it becomes evident that the evolution of  $\mathcal{D}(\omega \in \mathbb{C}; t)$  exhibits two distinct limiting behaviors, as shown in Fig. 2 (d3) and (e3), which coincide with the corresponding OBC and PBC spectra, respectively.

**Application to the non-Bloch response: eigenstate**— Secondly, we discuss detecting non-Hermitian eigenstates. For any given eigenvalue  $E_n$ , the right and left eigenstates,  $|\psi_n^R\rangle$  and  $\langle\psi_n^L|$  satisfy  $H_{\text{NH}}|\psi_n^R\rangle = E_n|\psi_n^R\rangle$  and  $\langle\psi_n^L|H_{\text{NH}} = \langle\psi_n^L|E_n$ , respectively. In Appendix E, it will be shown that

$$\lim_{t \rightarrow \infty} \lim_{\omega \rightarrow E_n} \mathcal{G}_{ij}(\omega; t) \sim \langle i | \psi_n^R \rangle \langle \psi_n^L | j \rangle. \quad (16)$$

By selecting any given site  $i_0$ , the components of the right and left eigenstates are detected via  $\mathcal{G}_{i_0 i_0}(\omega \rightarrow E_n; \infty) \propto \langle i | \psi_n^R \rangle$  and  $\mathcal{G}_{i_0 i}(\omega \rightarrow E_n; \infty) \propto \langle \psi_n^L | i \rangle$ , respectively. Importantly, the above conclusion is independent of  $i_0$  if  $\omega$  is sufficiently near  $E_n$ .

To exemplify the detection, the chosen Hamiltonian is

$$H_{\text{NH}}(\mathbf{k}) = \mathbf{d}(\mathbf{k}) \cdot \boldsymbol{\sigma} - i(\gamma_0 \sigma_0 + \gamma_z \sigma_z)/2, \quad (17)$$

where  $\boldsymbol{\sigma} = (\sigma_x, \sigma_y, \sigma_z)$  and  $\mathbf{d}(\mathbf{k}) = (t_1 \sin k_x, 2t_1 \sin k_y, \mu_z + t_2 \cos k_x + 2t_2 \cos k_y)$ . In this model, the emergence of the NHSE depends on the choice of OBC geometry [30, 37, 38, 59, 98–100]. Focusing on our study, we analyze the dia-

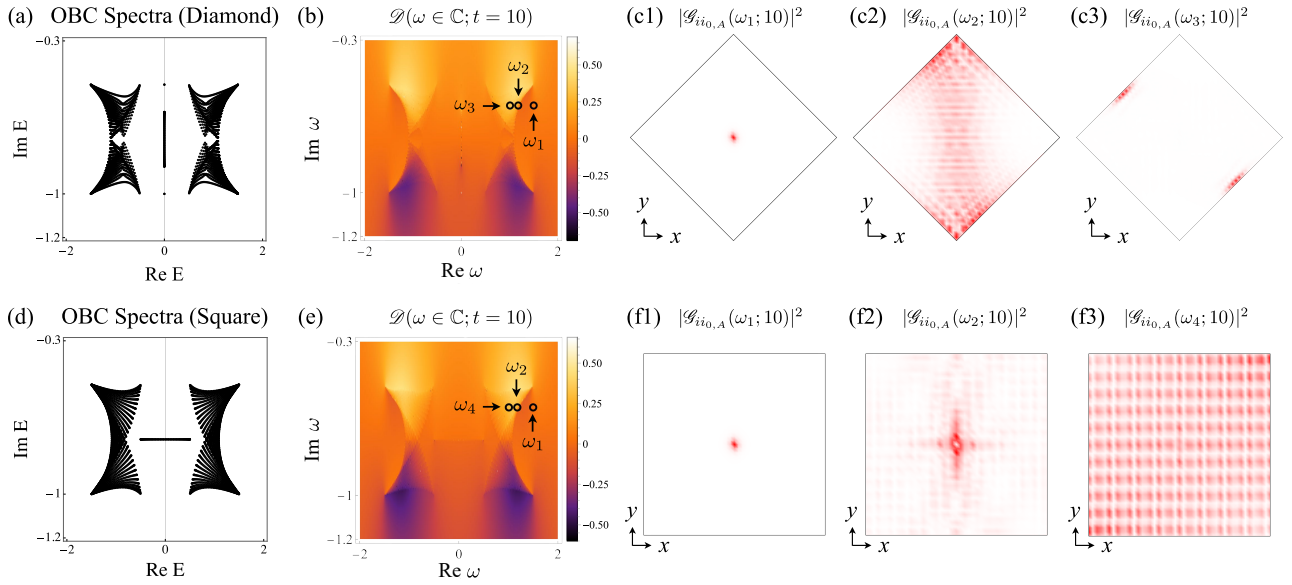


FIG. 3. (a)-(c) The OBC spectra,  $\mathcal{D}(\omega; t = 10)$ , and  $|\mathcal{G}_{ii_0,A}(\omega = \omega_1, \omega_2, \omega_3; 10)|^2$  for the diamond geometry of the Hamiltonian Eq. 17. Here  $\omega_3$  is chosen to be near the OBC eigenvalue and  $i_0$  denoting the central site. The system's size is  $L_x = L_y = 63$ . (d)-(f) The OBC spectra,  $\mathcal{D}(\omega; t = 10)$ , and  $|\mathcal{G}_{ii_0,A}(\omega = \omega_1, \omega_2, \omega_4; 10)|^2$  for the square geometry of the Hamiltonian Eq. 17. Here  $\omega_4$  is chosen to be near the OBC eigenvalue, and the system's size is  $L_x = L_y = 45$ . The parameters are selected as  $t_1 = t_2 = 0.5, \gamma_0 = 1.5, \gamma_z = -0.5, \omega_0 = 0, \mu_z = 0, \omega_1 = 1.5 - 0.6i, \omega_2 = 1.18 - 0.6i, \omega_3 = 1.01 - 0.6i$ , and  $\omega_4 = 1 - 0.603i$ .

mond and square geometries, with corresponding spectra depicted in Fig. 3 (a) and (d), respectively. Notably, the spectra are effectively characterized by  $\mathcal{D}(\omega; t = 10)$ , as shown in Fig. 3 (b) and (e). To detect the eigenstates corresponding to specific eigenvalues, we introduce  $|\mathcal{G}_{ij_A}(\omega; t)|^2 = |\mathcal{G}_{i_A j_A}(\omega; t)|^2 + |\mathcal{G}_{i_B j_A}(\omega; t)|^2$  for the two-band model. The results of  $|\mathcal{G}_{ii_0,A}(\omega_1 \sim \omega_4; 10)|^2$  are presented in Fig. 3 (c1)-(c3) and (f1)-(f3), with  $\omega_1$  to  $\omega_4$  chosen as indicated in Fig. 3 (b) and (e), and  $i_0$  selected as the central site in both the diamond and square geometries. From Fig. 3 (c) and (f), it can be observed that as  $\omega$  approaches the OBC eigenvalues, i.e.,  $\omega_3$  for (c) and  $\omega_4$  for (d), the corresponding eigenstate exhibits the skin mode for the diamond geometry and the Bloch mode for the square geometry.

**Application to the non-Bloch response: complex frequency LDOS**—Finally, the complex frequency LDOS can also be detected via the CFF as follows:

$$\lim_{t \rightarrow \infty} \mathcal{G}_{ii}(\omega \in \mathbb{C}; t) = D_{ii}(\omega \in \mathbb{C}). \quad (18)$$

Subsequently, we will apply this method to detect the point gap bound state [101]. The non-Hermitian Hamiltonian is given by

$$H_{\text{nh}}(k) = (t_1 + t_2 \cos k) \sigma_x + t_2 \sin k \sigma_y + (\lambda \sin k + \mu) \sigma_z + (t_3 \cos 2k) \sigma_0 - i(\gamma_0 \sigma_0 + \gamma_z \sigma_z) / 2. \quad (19)$$

Impurities are introduced as

$$V_I = V \sum_{i\alpha} \delta_{i1} |i, \alpha\rangle \langle i, \alpha|. \quad (20)$$

The OBC spectra and the complex frequency LDOS are depicted in Fig. 4 (a) and (b), respectively, vividly demonstrating the existence of a point gap bound state on the complex frequency plane.

**Conclusions and discussions.**—In summary, we have established a theoretical framework for detecting the complex frequency Green's function and the corresponding non-Bloch responses in driven dissipative systems based on the concept of the CFF. Through numerical simulations, we have successfully demonstrated the detectability of non-Hermitian eigenvalues, eigenstates, and impurity bound states using the CFF method, indicating its practical feasibility in experimental setups. Moreover, it is worth mentioning that even in cases

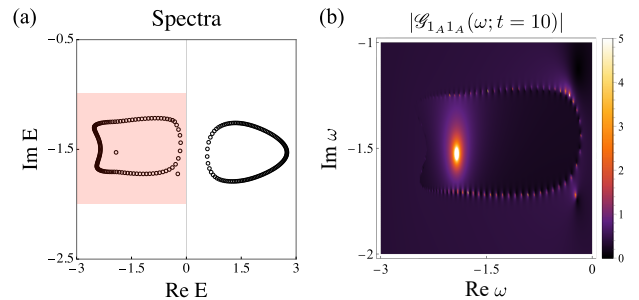


FIG. 4. (a) The PBC spectra of Eq. 19 with the presence of impurities. (b) The complex frequency LDOS, which is expressed as  $|\mathcal{G}_{1A1A}(\omega; t = 10)|$ . Here the parameters are set as  $t_1 = 1, t_2 = 1.6, \mu = 0.1, \gamma_0 = 3, \gamma_z = 1, \lambda = 1, t_3 = 0.5, V = 4, \omega_0 = 0$  and  $N = 120$ .

where the Hamiltonian exhibits frequency dependency, our theory remains applicable. Further elaboration on this aspect will be reserved for our upcoming research.

J. Huang. and Z. Yang were sponsored by the National Key R&D Program of China (No. 2023YFA1407500), the National Natural Science Foundation of China (No. 12322405, 12104450, 12047503). K. Ding was sponsored by the National Natural Science Foundation of China (No. 12174072, 2021hwyq05) and the National Key R&D Program of China (No. 2022YFA1404500, 2022YFA1404701). J. Hu was sponsored by the Ministry of Science and Technology (Grant No. 2022YFA1403901), National Natural Science Foundation of China (No. 11920101005, No. 11888101, No. 12047503, No. 12322405, No. 12104450) and the New Cornerstone Investigator Program.

## APPENDIX A: THE NON-BLOCH RESPONSE OF GREEN'S FUNCTIONS

This section provides a concise verification that a nonzero winding number will lead to the non-Bloch response of the Green's function, aligning with the conclusions presented in Fig. 1.

To examine the Green's function, we introduce  $\beta = e^{ik}$  and label  $\beta_{n=1,\dots,2M}$  as the roots of  $\det[\omega - H(\beta)] = \frac{P(\beta,\omega)}{\beta^M} = 0$ , with  $M = 2$  in our one-dimensional two-band model. For a given complex frequency  $\omega$ , the roots can be ordered as  $|\beta_1(\omega)| \leq |\beta_2(\omega)| \leq |\beta_3(\omega)| \leq |\beta_4(\omega)|$ , where  $\beta_1, \beta_2$  are enclosed by the generalized Brillouin Zone [76, 77]. The scaling behavior of the Green's function under OBC is described as [76, 77]

$$[G_{\text{OBC}}]_{i_\alpha, i_0, \beta} \sim \begin{cases} \beta_3^{-(i_0-i)}, & i < i_0 \\ \beta_2^{i-i_0}, & i > i_0 \end{cases} \quad (21)$$

for large  $|i - i_0|$ , where  $\alpha$  and  $\beta$  represent orbital indices. Besides, the roots can be alternatively ordered as  $|\beta_1(\omega)| \leq \dots \leq |\beta_\alpha(\omega)| \leq 1 \leq |\beta_4(\omega)|$ , then the result under PBC can be qualitatively characterized as [76, 77]

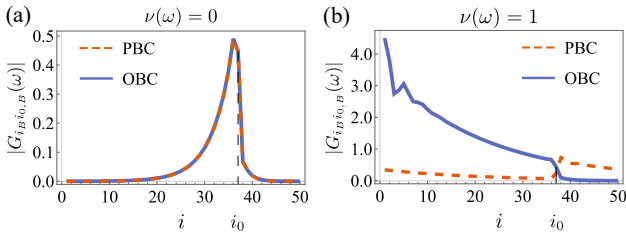


FIG. 5. (a)  $|G_{i_B i_0, B}(\omega)|$  for  $\nu(\omega) = 0$ , satisfying  $G_{\text{OBC}} \simeq G_{\text{PBC}}$ . Here  $\omega = 1.3 - i$  (b)  $|G_{i_B i_0, B}(\omega)|$  for  $\nu(\omega) = 1$ , satisfying  $G_{\text{OBC}} \neq G_{\text{PBC}}$ . Here  $\omega = 1.3 - 1.35i$ . In (a) and (b)  $i_0 = 37$ , all other parameters are identical to those used in Fig. 2.

$$[G_{\text{PBC}}]_{i_\alpha, i_0, \beta} \sim \begin{cases} \beta_{a+1}^{-(i_0-i)}, & i < i_0 \\ \beta_a^{i-i_0}, & i > i_0 \end{cases} \quad (22)$$

for large  $|i - i_0|$ , assuming  $|i - i_0|$  is away from the balanced point [76].

We now numerically demonstrate the conclusion presented in Fig. 1. The Hamiltonian considered is the spinless Rice-Mele model:  $H_{\text{NH}}(k) = (t_1 + t_2 \cos k)\sigma_x + t_2 \sin k \sigma_y + (\lambda \sin k + \mu)\sigma_z - i(\gamma_0 \sigma_0 + \gamma_z \sigma_z)/2$ , with the corresponding spectra illustrated in Fig. 2(a). The winding number is given by [97]

$$\nu(\omega) = \frac{1}{2\pi i} \int_0^{2\pi} dk \partial_k \ln \det[H_{\text{NH}}(k) - \omega]. \quad (23)$$

When  $\omega$  is outside the point gap, the roots satisfy  $|\beta_1(\omega)| \leq |\beta_2(\omega)| < 1 < |\beta_3(\omega)| \leq |\beta_4(\omega)|$  [76, 77]. Hence, the inequalities  $|\beta_2(\omega)| < 1$  and  $|\beta_3(\omega)| > 1$  hold for all  $\nu(\omega) = 0$ . In this case, we conclude that the scaling behavior of OBC Green's function will exponentially decay as  $i$  moves away  $i_0$ . It is evident that the scaling behavior of  $[G_{\text{PBC}}]_{i_\alpha, i_0, \beta}$  is identical to that of  $G_{\text{OBC}}$  since  $a = 2$  as shown in Eq. 22. Specifically, they coalesce, i.e.  $G_{\text{OBC}} \simeq G_{\text{PBC}}$  as depicted in Fig. 5 (a), corresponding to the Bloch response. A corollary can be drawn that for any  $\omega_0 \in \mathbb{R}$ , we still have  $G_{\text{OBC}}(\omega_0) \simeq G_{\text{PBC}}(\omega_0)$  as shown in Fig. 1.

When  $\omega$  is inside the point gap, i.e.  $\nu(\omega) = 1$ , we can deduce that  $|\beta_3(\omega)| < 1$ , indicating that the OBC Green's function exhibits universal decay as  $i$  increases. Conversely, the PBC Green's function still exhibits decaying behavior as  $i$  moves away from  $i_0$  since now  $a = 3$  as shown in Eq. 22, with  $|\beta_4(\omega)| > 1$ . This distinction is exemplified as shown in Fig. 5 (b), corresponding to the non-Bloch response, i.e.  $G_{\text{OBC}} \neq G_{\text{PBC}}$  as depicted in Fig. 1.

## APPENDIX B: DERIVATION OF THE EQUATION OF MOTION

This section provides a concise derivation of the equation of motion, namely Eq. 3. According to the quantum master equation Eq. 1, we obtain

$$\begin{aligned} i \frac{d\langle \hat{a}_m(t) \rangle}{dt} &= i \text{Tr} \left[ \hat{a}_m \frac{d\hat{\rho}(t)}{dt} \right] \\ &= i \text{Tr} \left[ \hat{a}_m \left( -i[\hat{H}(t), \hat{\rho}(t)] + \sum_{j=1}^N \kappa_j \hat{\mathcal{L}}_j[\hat{\rho}(t)] \right) \right] \\ &= \text{Tr} \left[ \hat{a}_m [\hat{H}(t), \hat{\rho}(t)] \right] + i \text{Tr} \left[ \hat{a}_m \sum_j \kappa_j \hat{\mathcal{L}}_j[\hat{\rho}(t)] \right]. \end{aligned} \quad (24)$$

We then employ the identity:

$$\text{Tr} \left[ \hat{a}_m [\hat{H}(t), \hat{\rho}(t)] \right] = \text{Tr} \left[ [\hat{a}_m, \hat{H}(t)] \hat{\rho}(t) \right]. \quad (25)$$

Subsequently, utilizing the bosonic commutation relation  $[\hat{a}_i, \hat{a}_j] = \delta_{ij}$ , we arrive at

$$[\hat{a}_m, \hat{H}(t)] = \sum_n t_{mn} \hat{a}_n + F_m(t). \quad (26)$$

Since  $\text{Tr}[\hat{\rho}(t)] = 1$ , we deduce

$$\text{Tr}[\hat{\mathbf{a}}, [\hat{H}(t), \hat{\rho}(t)]] = H_0 \langle \hat{\mathbf{a}}(t) \rangle + \mathbf{F}(t), \quad (27)$$

where  $[H_0]_{mn} = t_{mn}$  is the Hermitian Hamiltonian and  $\langle \hat{\mathbf{a}}(t) \rangle = \{\text{Tr}[\hat{a}_1 \hat{\rho}(t)], \dots, \text{Tr}[\hat{a}_N \hat{\rho}(t)]\}^T$ . Then by applying the identity

$$\begin{aligned} & \text{Tr}[\hat{a}_m (\hat{a}_j \hat{\rho}(t) \hat{a}_j^\dagger - \frac{1}{2} \{\hat{a}_j^\dagger \hat{a}_j, \hat{\rho}(t)\})] \\ &= \text{Tr}[(\hat{a}_j^\dagger \hat{a}_m \hat{a}_j - \frac{1}{2} \{\hat{a}_m, \hat{a}_j^\dagger \hat{a}_j\}) \hat{\rho}(t)] \\ &= \text{Tr}[\frac{1}{2} (\hat{a}_j^\dagger, \hat{a}_m) \hat{a}_j + \hat{a}_j^\dagger [\hat{a}_m, \hat{a}_j] \hat{\rho}(t)] \\ &= -\frac{1}{2} \delta_{mj} \langle \hat{a}_j(t) \rangle, \end{aligned} \quad (28)$$

we derive

$$i \text{Tr}[\hat{a}_m \sum_j \kappa_j \hat{\mathcal{L}}_j [\hat{\rho}(t)]] = -\frac{i}{2} \kappa_m \langle \hat{a}_m(t) \rangle. \quad (29)$$

Consequently, we establish

$$i \frac{d \langle \hat{\mathbf{a}}(t) \rangle}{dt} = H_{\text{nH}} \langle \hat{\mathbf{a}}(t) \rangle + \mathbf{F}(t), \quad (30)$$

with  $[H_{\text{nH}}]_{mn} = t_{mn} - \frac{i}{2} \kappa_m \delta_{mn}$  denoting the non-Hermitian Hamiltonian in the first quantized form.

### APPENDIX C: DERIVATION OF THE RESPONSE FUNCTION

This section provides a brief derivation of the solution for  $\chi_{\omega_0}(t)$ . It is easy to check that the general solution of Eq. 3 is expressed as

$$\langle \hat{\mathbf{a}}(t) \rangle = e^{-iH_{\text{nH}}t} [-i \int_0^t e^{iH_{\text{nH}}\tau} \mathbf{F}_{\omega_0}(\tau) d\tau + \langle \hat{\mathbf{a}}(0) \rangle]. \quad (31)$$

Considering a harmonic external driving  $\mathbf{F}_{\omega_0}(t) = \theta(t) e^{-i\omega_0 t} \{F_1(0), \dots, F_N(0)\}^T$  with  $\theta(t)$  representing the step function, a straightforward integral over  $\tau$  yields:

$$\begin{aligned} \langle \hat{\mathbf{a}}(t) \rangle &= e^{-iH_{\text{nH}}t} [-i \int_0^t e^{iH_{\text{nH}}\tau} \mathbf{F}_{\omega_0}(\tau) d\tau + \langle \hat{\mathbf{a}}(0) \rangle] \\ &= \frac{e^{-i\omega_0 t} - e^{-iH_{\text{nH}}t}}{\omega_0 - H_{\text{nH}}} \theta(t) \{F_1(0), \dots, F_N(0)\}^T \\ &+ e^{-iH_{\text{nH}}t} \langle \hat{\mathbf{a}}(0) \rangle \\ &= G(\omega_0) (1 - e^{-i(H_{\text{nH}} - \omega_0)t}) \mathbf{F}_{\omega_0}(t) \\ &+ e^{-i(H_{\text{nH}} - \omega_0)t} \text{Diag}(\frac{\langle \hat{a}_1(0) \rangle}{F_1(0)}, \dots, \frac{\langle \hat{a}_N(0) \rangle}{F_N(0)}) \mathbf{F}_{\omega_0}(t), \end{aligned} \quad (32)$$

where  $G(\omega_0) = \frac{1}{\omega_0 - H_{\text{nH}}}$  and  $\text{Diag}(\dots)$  denotes the diagonal matrix. Subsequently, the response function is determined as:

$$\langle \hat{\mathbf{a}}(t) \rangle_{\omega_0} = \chi_{\omega_0}(t) \mathbf{F}_{\omega_0}(t), \quad (33)$$

with

$$\begin{aligned} [\chi_{\omega_0}(t)]_{mn} &= [G(\omega_0)]_{mn} - [G(\omega_0) e^{-i(H_{\text{nH}} - \omega_0)t}]_{mn} \\ &+ [e^{-i(H_{\text{nH}} - \omega_0)t}]_{mn} \langle \hat{a}_n(0) \rangle / F_n(0). \end{aligned} \quad (34)$$

To simplify the discussion in the main text, we assume that  $\langle \hat{\mathbf{a}}(0) \rangle = 0$ , a condition that does not impact our qualitative findings.

### APPENDIX D: DETECTION OF THE COMPLEX FREQUENCY DOS

In this section, we illustrate the methodology for detecting the density of states through the CFF method. The decent definition of DOS on the complex energy plane is given by

$$\rho(\omega) = \frac{1}{N} \sum_n \delta(\text{Re } \omega - \text{Re } E_n) \delta(\text{Im } \omega - \text{Im } E_n), \quad (35)$$

where  $E_n$  denotes the  $n$ -th eigenvalue of the non-Hermitian Hamiltonian  $H_{\text{nH}}$ . To establish a connection between this definition and the Green's function, the generalization for DOS should be as follows [102–105]:

$$\begin{aligned} \rho(\omega) &= \frac{1}{\pi N} \frac{\partial}{\partial \omega^*} \text{Tr } G(\omega) \\ &= \frac{1}{\pi N} \sum_n \frac{\partial}{\partial \omega^*} \frac{1}{\omega - E_n}. \end{aligned} \quad (36)$$

By using the identity

$$\begin{aligned} \delta(\omega - E_n) &= \delta(\text{Re } \omega - \text{Re } E_n) \delta(\text{Im } \omega - \text{Im } E_n) \\ &= \frac{1}{\pi} \frac{\partial}{\partial \omega^*} \frac{1}{\omega - E_n}, \end{aligned} \quad (37)$$

we arrive at Eq. 35, with  $\int_{-\infty}^{\infty} d \text{Re } \omega \int_{-\infty}^{\infty} d \text{Im } \omega \rho(\omega) = 1$ . To validate Eq. 35 numerically, it is essential to introduce two parameters,  $\eta_r$  and  $\eta_i$ , to simulate the Dirac delta function using the relation  $\delta(x) = -\frac{1}{\pi} \text{Im} \frac{1}{x+i\eta}$ . However, Eq. 35 is not directly linked to the complex frequency Green's function; therefore, we shift our attention to Eq. 36.

Although we have derived the formula Eq. 36 for the DOS in the complex energy plane, direct application is not feasible. Notably,  $\rho(\omega = E_n)$  is divergent, rendering the ill-defined partial differential form at  $\omega = E_n$ . This contrasts with the real-frequency case, where the pole of  $\rho(\omega \in \mathbb{R}) \sim \frac{1}{\omega - E + i\eta}$  on the real axis is circumvented by the parameter  $\eta$ . However, the poles in the complex energy plane can not be circumvented by introducing complex parameters. Therefore Eq. 36 cannot be directly applied in experiments.

Moreover, we note that the qualitative validity of Eq. 36 originates from its resemblance to the Maxwell equation of

the electric field in the  $xy$  plane. In the realm of electrodynamics, the electric field  $\mathbf{E}$  generated by an infinite line of charge along the  $z$ -axis is solely dependent on  $x$  and  $y$  [106]:

$$\begin{aligned}\mathbf{E} &= \frac{q}{2\pi\epsilon_0} \frac{x\mathbf{i} + y\mathbf{j}}{x^2 + y^2} \\ \nabla \cdot \mathbf{E} &= \frac{\rho_q}{\epsilon_0} = \frac{q}{\epsilon_0} \delta(x)\delta(y),\end{aligned}\quad (38)$$

where  $\rho_q$  signifies the density of the line of charge  $q$  and  $\epsilon_0$  denotes the vacuum permittivity. Similarly, a pole-field  $\mathcal{E}$  can be introduced in the complex plane:

$$\mathcal{E} = \frac{1}{2\pi N} (\text{Re Tr } G(\omega), \text{Im Tr } G(\omega)). \quad (39)$$

The contribution of a pole  $E_n$  to the pole-field is

$$\mathcal{E}_n = \frac{1}{2\pi N} \frac{(\text{Re } \omega - \text{Re } E_n, \text{Im } \omega - \text{Im } E_n)}{|\omega - E_n|^2}, \quad (40)$$

mirroring the form of the electric field  $\mathbf{E}$  due to a line of charge. By utilizing the identity  $\partial_{\omega^*} = \frac{1}{2}(\partial_{\text{Re } \omega} + i\partial_{\text{Im } \omega})$ , Eq. 36 transforms into

$$\begin{aligned}\rho(\omega) &= \nabla_{\omega} \cdot \mathcal{E} \\ &= \frac{1}{N} \sum_n \delta(\text{Re } \omega - \text{Re } E_n) \delta(\text{Im } \omega - \text{Im } E_n),\end{aligned}\quad (41)$$

where  $\nabla_{\omega} = (\partial_{\text{Re } \omega}, \partial_{\text{Im } \omega})$ . Here, the eigenvalues  $E_i, i = 1, 2, \dots, N$  corresponds to the positions of  $N$  lines of charge. Additionally, the pole potential can be introduced as [107]

$$\mathcal{V}(\omega) = -\frac{1}{2\pi N} \sum_n \ln |\omega - E_n|, \quad (42)$$

satisfying  $\mathcal{E} = -\nabla_{\omega} \mathcal{V}(\omega)$ . Notably  $\mathcal{V}(\omega)$  possesses redundant degrees of freedom since a constant gauge transformation  $\mathcal{V}(\omega) \rightarrow \mathcal{V}(\omega) + f$  with  $\nabla_{\omega} f = 0$  is permissible. Consequently, the Laplacian of the pole-potential yields the generalized DOS on the complex energy plane

$$-\nabla_{\omega}^2 \mathcal{V}(\omega) = \rho(\omega). \quad (43)$$

Furthermore, it is observed that  $\mathcal{V}(\omega)$  can be correlated with the Green's function at complex frequencies via

$$\mathcal{V}(\omega) = \frac{1}{2\pi N} \ln |\det G(\omega)|. \quad (44)$$

Therefore, the pole potential can be utilized to detect the DOS through the above formula. Specifically, using the CFF we can define the time-dependent pole-potential as

$$\mathcal{V}_{\omega_0}(\omega; t) = \frac{1}{2\pi N} \ln |\det \mathcal{G}_{\omega_0}(\omega; t)|, \quad (45)$$

and  $-\nabla_{\omega}^2 \mathcal{V}_{\omega_0}(\omega; \infty)$  provides the desired DOS in the complex energy plane.

Furthermore, considering the cumbersome numerical procedure involved in computing a Laplacian, an alternative formula for detecting the complex frequency DOS is proposed in the main text as shown in Eq. 11 and Eq. 12. Besides, it holds a significant physical interpretation as the  $y$  component of the pole field once the system reaches a stationary state, i.e. when  $t > t_s$ , where  $t_s \sim |\frac{1}{\text{Im } E_s}|$  with  $E_s$  representing the closest eigenvalue of  $H_{\text{NH}}$  to the real axis.

## APPENDIX E: DETECTION OF OBC EIGENSTATES

In this section, we demonstrate how the OBC eigenstates can be detected using the CFF method. By using the biorthogonal basis, the OBC eigenstates are related to the Green's function through the expression

$$G(\omega) = \sum_m \frac{|\psi_m^R\rangle \langle \psi_m^L|}{\omega - E_m}, \quad (46)$$

where  $|\psi_m^{R/L}\rangle$  represents the  $m$ -th right/left eigenstate. Thus, as  $\omega$  approaches an eigenvalue, such as  $E_n$ , the corresponding correlation can precisely reveal the eigenstate as shown by

$$G_{ij}(\omega \rightarrow E_n) \sim \frac{\langle i|\psi_n^R\rangle \langle \psi_n^L|j\rangle}{\omega - E_n}. \quad (47)$$

Furthermore, when fixing a site  $i = i_0$ , then the responses  $G_{i_0 i_0}(\omega \rightarrow E_n)$  and  $G_{i_0 i}(\omega \rightarrow E_n)$  are proportional to the  $i$ -th component of the right and left eigenstates, respectively. Consequently, since  $\mathcal{G}_{\omega_0}(E_n; t \rightarrow \infty) = G(\omega \rightarrow E_n)$ , the eigenstates can be detected by using the CFF method:

$$\lim_{t \rightarrow \infty} \mathcal{G}_{ij}(E_n; t) \sim \langle i|\psi_n^R\rangle \langle \psi_n^L|j\rangle, \quad (48)$$

where the subscript  $\omega_0$  is omitted for simplicity since the choice of  $\omega_0$  is irrelevant to the final outcome. In conclusion, we can detect the eigenstates through  $\mathcal{G}_{i_0 i_0}(E_n; t \rightarrow \infty) \propto \langle i|\psi_n^R\rangle$  and  $\mathcal{G}_{i_0 i}(E_n; t \rightarrow \infty) \propto \langle \psi_n^L|i\rangle$ , and the results are independent of the chosen site  $i_0$ .

\* Corresponding author: [jphu@iphy.ac.cn](mailto:jphu@iphy.ac.cn)

† Corresponding author: [yangzs@xmu.edu.cn](mailto:yangzs@xmu.edu.cn)

- [1] Y. Ashida, Z. Gong, and M. Ueda, *Adv. Phys.* **69**, 249 (2020).
- [2] L. E. F. F. Torres, *JPhys mater.* **3**, 014002 (2019).
- [3] R. Lin, T. Tai, L. Li, and C. H. Lee, *Front. Phys.* **18**, 53605 (2023).
- [4] E. J. Bergholtz, J. C. Budich, and F. K. Kunst, *Rev. Mod. Phys.* **93**, 015005 (2021).
- [5] S. Yao and Z. Wang, *Phys. Rev. Lett.* **121**, 086803 (2018).
- [6] V. M. Martinez Alvarez, J. E. Barrios Vargas, and L. E. F. Foa Torres, *Phys. Rev. B* **97**, 121401 (2018).
- [7] F. K. Kunst, E. Edvardsson, J. C. Budich, and E. J. Bergholtz, *Phys. Rev. Lett.* **121**, 026808 (2018).
- [8] T. E. Lee, *Phys. Rev. Lett.* **116**, 133903 (2016).
- [9] Y. Xiong, *J. Phys. Commun.* **2**, 035043 (2018).

- [10] L. Jin and Z. Song, *Phys. Rev. B* **99**, 081103 (2019).
- [11] K. Kawabata, K. Shiozaki, M. Ueda, and M. Sato, *Phys. Rev. X* **9**, 041015 (2019).
- [12] X. Zhang, T. Zhang, M.-H. Lu, and Y.-F. Chen, *Adv. Phys. X* **7**, 2109431 (2022).
- [13] S. Weidemann, M. Kremer, T. Helbig, T. Hofmann, A. Stegmaier, M. Greiter, R. Thomale, and A. Szameit, *Science* **368**, 311 (2020).
- [14] L. Xiao, T.-S. Deng, K. Wang, G. Zhu, Z. Wang, W. Yi, and P. Xue, *Nat. Phys.* **16**, 761 (2020).
- [15] C. R. Leefmans, M. Parto, J. Williams, G. H. Y. Li, A. Dutt, F. Nori, and A. Marandi, *Nat. Phys.* **20**, 852 (2024).
- [16] Q. Lin, T. Li, L. Xiao, K. Wang, W. Yi, and P. Xue, *Nat. Commun.* **13**, 3229 (2022).
- [17] Z. Lin, W. Song, L.-W. Wang, H. Xin, J. Sun, S. Wu, C. Huang, S. Zhu, J.-H. Jiang, and T. Li, *Phys. Rev. Lett.* **133**, 073803 (2024).
- [18] L. Xiao, W.-T. Xue, F. Song, Y.-M. Hu, W. Yi, Z. Wang, and P. Xue, *Phys. Rev. Lett.* **133**, 070801 (2024).
- [19] G.-G. Liu, S. Mandal, P. Zhou, X. Xi, R. Banerjee, Y.-H. Hu, M. Wei, M. Wang, Q. Wang, Z. Gao, H. Chen, Y. Yang, Y. Chong, and B. Zhang, *Phys. Rev. Lett.* **132**, 113802 (2024).
- [20] Y. Sun, X. Hou, T. Wan, F. Wang, S. Zhu, Z. Ruan, and Z. Yang, *Phys. Rev. Lett.* **132**, 063804 (2024).
- [21] Z. Gao, X. Qiao, M. Pan, S. Wu, J. Yim, K. Chen, B. Midya, L. Ge, and L. Feng, *Phys. Rev. Lett.* **130**, 263801 (2023).
- [22] Q. Lin, T. Li, L. Xiao, K. Wang, W. Yi, and P. Xue, *Phys. Rev. Lett.* **129**, 113601 (2022).
- [23] M. Gao, C. Sheng, Y. Zhao, R. He, L. Lu, W. Chen, K. Ding, S. Zhu, and H. Liu, *Phys. Rev. B* **110**, 094308 (2024).
- [24] S. Wang, B. Wang, C. Liu, C. Qin, L. Zhao, W. Liu, S. Longhi, and P. Lu, [arXiv:2409.19693](https://arxiv.org/abs/2409.19693).
- [25] R. A. Vicencio, D. Román-Cortés, M. Rubio-Saldías, P. Vildoso, and L. E. F. F. Torres, [arXiv:2407.18174](https://arxiv.org/abs/2407.18174).
- [26] L. Zhang, Y. Yang, g. Yong, G. Jun, Q. Chen, Q. Yan, F. Chen, R. Xi, Y. Li, D. Jia, S.-Q. Yuan, H.-x. Sun, H. Chen, and B. Zhang, *Nat. Commun.* **12**, 6297 (2021).
- [27] Z. Gu, H. Gao, H. Xue, J. Li, Z. Su, and J. Zhu, *Nat. Commun.* **13**, 7668 (2022).
- [28] H. Gao, H. Xue, Z. Gu, L. Li, W. Zhu, Z. Su, J. Zhu, B. Zhang, and Y. D. Chong, *Phys. Rev. B* **106**, 134112 (2022).
- [29] X. Zhang, Y. Tian, J.-H. Jiang, M.-H. Lu, and Y.-F. Chen, *Nat. Commun.* **12**, 5377 (2021).
- [30] Q. Zhou, J. Wu, Z. Pu, J. Lu, X. Huang, W. Deng, M. Ke, and Z. Liu, *Nat. Commun.* **14**, 4569 (2023).
- [31] J. Wu, R. Zheng, J. Liang, M. Ke, J. Lu, W. Deng, X. Huang, and Z. Liu, *Phys. Rev. Lett.* **133**, 126601 (2024).
- [32] L. Xiong, Q. Zhang, X. Feng, Y. Leng, M. Pi, S. Tong, and C. Qiu, *Phys. Rev. B* **110**, L140305 (2024).
- [33] Q. Zhang, Y. Leng, L. Xiong, Y. Li, K. Zhang, L. Qi, and C. Qiu, *Adv. Mater.* **36**, 2403108 (2024).
- [34] H. Gao, W. Zhu, H. Xue, G. Ma, and Z. Su, *Appl. Phys. Rev.* **11**, 031410 (2024).
- [35] J.-X. Zhong, P. F. de Castro, T. Lu, J. Kim, M. Oudich, J. Ji, L. Shi, K. Chen, J. Lu, Y. Jing, and W. A. Benalcazar, [arXiv:2409.01516](https://arxiv.org/abs/2409.01516).
- [36] B. bing Wang, Z. Cheng, H. yu Zou, Y. Ge, K. qi Zhao, Q. rui Si, S. qi Yuan, H. xiang Sun, H. Xue, and B. Zhang, [arXiv:2402.10989](https://arxiv.org/abs/2402.10989).
- [37] Y. Hu, J. Wu, P. Ye, W. Deng, J. Lu, X. Huang, Z. Wang, M. Ke, and Z. Liu, [arXiv:2407.03868](https://arxiv.org/abs/2407.03868).
- [38] T. Wan, K. Zhang, J. Li, Z. Yang, and Z. Yang, *Sci. Bull.* **68**, 2330 (2023).
- [39] Q. Liang, D. Xie, Z. Dong, H. Li, H. Li, B. Gadway, W. Yi, and B. Yan, *Phys. Rev. Lett.* **129**, 070401 (2022).
- [40] E. Zhao, Z. Wang, C. He, T. F. J. Poon, K. K. Pak, Y.-J. Liu, P. Ren, X.-J. Liu, and G.-B. Jo, [arXiv:2311.07931](https://arxiv.org/abs/2311.07931).
- [41] T. Helbig, T. Hofmann, S. Imhof, M. Abdelghany, T. Kiessling, L. Molenkamp, C. H. Lee, A. Szameit, M. Greiter, and R. Thomale, *Nat. Phys.* **16**, 747 (2020).
- [42] T. Hofmann, T. Helbig, F. Schindler, N. Salgo, M. Brzezińska, M. Greiter, T. Kiessling, D. Wolf, A. Vollhardt, A. Kabaši, C. H. Lee, A. Bilušić, R. Thomale, and T. Neupert, *Phys. Rev. Res.* **2**, 023265 (2020).
- [43] S. Liu, R. Shao, S. Ma, L. Zhang, O. You, H. Wu, Y. J. Xiang, T. J. Cui, and S. Zhang, *Research* **2021**, 5608038 (2021).
- [44] D. Zou, T. Chen, W. He, J. Bao, C. H. Lee, H. Sun, and X. Zhang, *Nat. Commun.* **12**, 7201 (2021).
- [45] W. Deng, T. Chen, and X. Zhang, *Phys. Rev. Res.* **4**, 033109 (2022).
- [46] C. Shang, S. Liu, R. Shao, P. Han, X. Zang, X. Zhang, K. Salama, W. Gao, C. H. Lee, R. Thomale, A. Manchon, S. Zhang, T. Cui, and U. Schwingenschlögl, *Adv. Sci.* **9**, 2202922 (2022).
- [47] H. Zhang, T. Chen, L. Li, C. H. Lee, and X. Zhang, *Phys. Rev. B* **107**, 085426 (2023).
- [48] L. Su, C.-X. Guo, Y. Wang, L. Li, X. Ruan, Y. Du, S. Chen, and D. Zheng, *Chinese Phys. B* **32**, 038401 (2023).
- [49] P. Zhu, X.-Q. Sun, T. Hughes, and G. Bahl, *Nat. Commun.* **14**, 720 (2023).
- [50] B. Liu, Y. Li, B. Yang, X. Shen, Y. Yang, Z. H. Hang, and M. Ezawa, *Phys. Rev. Res.* **5**, 043034 (2023).
- [51] C. Tang, H. Yang, L. Song, X. Yao, P. Yan, and Y. Cao, *Phys. Rev. B* **108**, 035410 (2023).
- [52] L. Su, H. Jiang, Z. Wang, S. Chen, and D. Zheng, *Phys. Rev. B* **107**, 184108 (2023).
- [53] W.-W. Jin, J. Liu, X. Wang, Y.-R. Zhang, X. Huang, X. Wei, W. Ju, T. Liu, Z. Yang, and F. Nori, [arXiv:2311.03777](https://arxiv.org/abs/2311.03777).
- [54] A. Ghatak, M. Brandenbourger, J. Wezel, and C. Coulais, *Proc. Natl. Acad. Sci. U.S.A.* **117**, 29561 (2020).
- [55] M. Brandenbourger, X. Locsin, E. Lerner, and C. Coulais, *Nat. Commun.* **10**, 1 (2019).
- [56] Y. Chen, X. Li, C. Scheibner, V. Vitelli, and G. Huang, *Nat. Commun.* **12**, 5935 (2021).
- [57] W. Wang, X. Wang, and G. Ma, *Nature* **608**, 50 (2022).
- [58] Z. Li, L.-W. Wang, X. Wang, Z.-K. Lin, G. Ma, and J.-H. Jiang, *Nat. Commun.* **15**, 6544 (2024).
- [59] W. Wang, M. Hu, X. Wang, G. Ma, and K. Ding, *Phys. Rev. Lett.* **131**, 207201 (2023).
- [60] A. Wang, Z. Meng, and C. Q. Chen, *Sci. Adv.* **9**, eadf7299 (2023).
- [61] S. Yao, F. Song, and Z. Wang, *Phys. Rev. Lett.* **121**, 136802 (2018).
- [62] T.-S. Deng and W. Yi, *Phys. Rev. B* **100**, 035102 (2019).
- [63] K. Yokomizo and S. Murakami, *Phys. Rev. Lett.* **123**, 066404 (2019).
- [64] K. Kawabata, N. Okuma, and M. Sato, *Phys. Rev. B* **101**, 195147 (2020).
- [65] Z. Yang, K. Zhang, C. Fang, and J. Hu, *Phys. Rev. Lett.* **125**, 226402 (2020).
- [66] H. Jiang and C. H. Lee, *Phys. Rev. Lett.* **131**, 076401 (2023).
- [67] C. H. Lee and R. Thomale, *Phys. Rev. B* **99**, 201103 (2019).
- [68] F. Song, S. Yao, and Z. Wang, *Phys. Rev. Lett.* **123**, 246801 (2019).
- [69] F. Song, S. Yao, and Z. Wang, *Phys. Rev. Lett.* **123**, 170401 (2019).
- [70] S. Longhi, *Phys. Rev. Res.* **1**, 023013 (2019).



- [71] K. Zhang, Z. Yang, and C. Fang, *Phys. Rev. Lett.* **125**, 126402 (2020).
- [72] C. H. Lee and S. Longhi, *Commun. Phys.* **3**, 147 (2020).
- [73] S. Longhi, *Phys. Rev. Lett.* **124**, 066602 (2020).
- [74] C. H. Lee, L. Li, R. Thomale, and J. Gong, *Phys. Rev. B* **102**, 085151 (2020).
- [75] M. Wu, Q. Zhao, L. Kang, M. Weng, Z. Chi, R. Peng, J. Liu, D. H. Werner, Y. Meng, and J. Zhou, *Phys. Rev. B* **107**, 064307 (2023).
- [76] W.-T. Xue, M.-R. Li, Y.-M. Hu, F. Song, and Z. Wang, *Phys. Rev. B* **103**, L241408 (2021).
- [77] Y.-M. Hu and Z. Wang, *Phys. Rev. Res.* **5**, 043073 (2023).
- [78] B. Ahmadi, P. Mazurek, P. Horodecki, and S. Barzanjeh, *Phys. Rev. Lett.* **132**, 210402 (2024).
- [79] H.-P. Breuer and F. Petruccione, *The Theory of Open Quantum Systems* (2006).
- [80] Á. Rivas and S. F. Huelga, *Open Quantum Systems* (2012).
- [81] C. Downing and M. Ukhtary, *Commun. Phys.* **6**, 322 (2023).
- [82] H. Haus and W. Huang, *Proc. IEEE*. **79**, 1505 (1991).
- [83] W.-P. Huang, *J. Opt. Soc. Am. A* **11**, 963 (1994).
- [84] Q. Li, T. Wang, Y. Su, M. Yan, and M. Qiu, *Opt. Express* **18**, 8367 (2010).
- [85] S. Fan, W. Suh, and J. D. Joannopoulos, *J. Opt. Soc. Am. A* **20**, 569 (2003).
- [86] W. Suh, Z. Wang, and S. Fan, *IEEE J. Quantum Electron.* **40**, 1511 (2004).
- [87] F. Guan, X. Guo, K. Zeng, S. Zhang, Z. Nie, S. Ma, Q. Dai, J. Pendry, X. Zhang, and S. Zhang, *Science* **381**, 766 (2023).
- [88] F. Guan, X. Guo, S. Zhang, K. Zeng, Y. Hu, C. Wu, S. Zhou, Y. J. Xiang, X. Yang, and S. Zhang, *Nat. Mater.* **23**, 506 (2024).
- [89] K. Zeng and S. Zhang, *Acta. Optica. Sinica.* **44**, 1026019 (2024).
- [90] H. Li, A. Mekawy, A. Krasnok, and A. Alù, *Phys. Rev. Lett.* **124**, 193901 (2020).
- [91] A. Archambault, M. Besbes, and J.-J. Greffet, *Phys. Rev. Lett.* **109**, 097405 (2012).
- [92] K. L. Tsakmakidis, T. W. Pickering, J. M. Hamm, A. F. Page, and O. Hess, *Phys. Rev. Lett.* **112**, 167401 (2014).
- [93] H. Tetikol and M. Aksun, *Plasmonics* **15**, 2137 (2020).
- [94] K. Tsakmakidis and M. Wartak, *Metamaterials and Nanophotonics: Principles, Techniques and Applications* (2022).
- [95] S. Kim, S. Lepeshov, A. Krasnok, and A. Alù, *Phys. Rev. Lett.* **129**, 203601 (2022).
- [96] S. Kim, Y.-G. Peng, S. Yves, and A. Alù, *Phys. Rev. X* **13**, 041024 (2023).
- [97] Y. Yi and Z. Yang, *Phys. Rev. Lett.* **125**, 186802 (2020).
- [98] K. Zhang, Z. Yang, and C. Fang, *Nat. Commun.* **13**, 2496 (2022).
- [99] Z. Fang, M. Hu, L. Zhou, and K. Ding, *Nanophotonics* **11**, 3447 (2022).
- [100] Y. Qin, K. Zhang, and L. Li, *Phys. Rev. A* **109**, 023317 (2024).
- [101] Z. Fang, C. Fang, and K. Zhang, *Phys. Rev. B* **108**, 165132 (2023).
- [102] S. Hikami and R. Prini, *J. Phys. A Math. Gen.* **31**, L587 (1998).
- [103] J. Feinberg and A. Zee, *Nucl. Phys. B.* **504**, 579 (1997).
- [104] H. J. Sommers, A. Crisanti, H. Sompolinsky, and Y. Stein, *Phys. Rev. Lett.* **60**, 1895 (1988).
- [105] F. Haake, F. Izrailev, N. Lehmann, D. SteinSaher, and H. J. Sommers, *Z. Phys. B* **88**, 359 (1992).
- [106] D. Griffiths, *Introduction to Electrodynamics* (2017).
- [107] Y. Xiong and H. Hu, *Phys. Rev. B* **109**, L100301 (2024).